ScienceDirect   Journals & Books   ⑦   Create account   Sign in   Top 25 Hottest Articl

≡ 📕 Download   Share   Export

Comparison of 35 and 50 μm thin HPK UFSD after neutron irradiation up to $6 \cdot 10^{15}$ neq/cm^2

Y. Zhao [a], N. Cartiglia [a, 1], E. Estrada [a], Z. Galloway [a], C. Gee [a], A. Goto [a], Z. Luce [a], S.M. Mazza [a] ✉, F. McKinney-Martinez [a], R. Rodriguez [a], H.F.-W. Sadrozinski [a], A. Seiden [a], V. Cindro [b], G. Kramberger [b], I. Mandić [b], M. Mikuž [b], M. Zavrtanik [b]

⊞ Show more

Get rights and content

Abstract

We report results from the testing of 35 μm thick Ultra-Fast Silicon Detectors (UFSD) produced by Hamamatsu Photonics (HPK), Japan and the comparison of these new results to data reported in a previous paper on 50 μm thick UFSD produced by HPK. The 35 μm thick sensors were irradiated with neutrons to fluences of $1 \cdot 10^{14}$, $1 \cdot 10^{15}$, $3 \cdot 10^{15}$, $6 \cdot 10^{15}$ neq/cm^2. The sensors were tested pre-irradiation and post-irradiation with minimum ionizing particles (MIPs) from a ^{90}Sr β-source. The leakage current, capacitance, internal gain and the timing resolution were measured as a function of bias voltage at –20 °C and –27 °C. The timing resolution was extracted from the time difference with a second calibrated UFSD in coincidence, using the constant fraction discrimination method for both devices. Within the fluence range measured, 35 μm thick UFSD present advantages in timing accuracy, bias voltage and power consumption.

< Previous   Next >

Keywords

Fast silicon sensors; Charge multiplication; Thin tracking sensors; Radiation damage; Time resolution

1. Introduction

Ultra-fast silicon detector (UFSD) are a new type of silicon detectors that will establish a new paradigm for space–time particle tracking [1]. These devices will ultimately measure with high precision concurrently space (~ 10 μm) and time ($\sim$10 ps) coordinates of a particle in a single device.

UFSD are silicon sensors based on the Low-Gain Avalanche Detector (LGAD) design [2], [3], [4] developed by the Centro Nacional de Microelectrónica (CNM) Barcelona, in part as a RD50 Common Project [5]. The main property of LGAD sensors is a moderate internal gain ($\sim$5–70) due to a highly doped p+ region just below the n-type implants. In the last years, the thickness of the LGAD were continually decreased from initial 300 μm down to 45 μm where a time resolution below 30 ps was achieved in a beam test with un-irradiated UFSD fabricated by CNM [6], [7], [8]. The measurements that were taken on several UFSDs agreed well with the predictions of the simulation program Weightfield2 (WF2) [9].

In the upgrades of the ATLAS and CMS experiments at the High-Luminosity Large Hadron Collider (HL-LHC [10]) UFSD will be employed as reviewed in [11]. The UFSD would be of moderate segmentation (around 1 mm^2 per pad) and will face challenging radiation requirements (fluences up to several 10^{15} neq/cm^2 and several hundred of MRad). Results on irradiated CNM LGAD 300 μm, 75 μm and 45 μm thick sensors were presented in [12], [13]. Recently, a radiation campaign with neutrons for 50 μm thick LGAD produced by Hamamatsu Photonics, Japan (HPK) has been reported [14]. In all cases the timing resolution has been shown to deteriorate with fluence due to the decreasing value of the gain. This effect is caused by the acceptor removal mechanism [15] that decreases the concentration of the active dopant in the gain layer. Since the data showed that a reduction of the sensor thickness leads to an improved time resolution, natural questions are the ultimate limit of the thickness of the sensor bulk and the optimized doping profile of the gain layer.

In this paper, we report on the performances of 35 μm thick UFSD produced by HPK before irradiation and after a neutron irradiation of fluences of $1 \cdot 10^{14}$, $4 \cdot 10^{14}$, $1 \cdot 10^{15}$, $3 \cdot 10^{15}$, $6 \cdot 10^{15}$ neq/cm^2. In Section 2 we will describe the characteristics of 35 μm thick UFSD, followed in Section 3 by a short description of the irradiation facility. In Section 4, a short description of the experimental set-up is presented, details were previously reported in [6], [14]. In Section 5, we will describe the data analysis including the extraction of the gain and the time resolution, and in Section 6 the results on bias dependence of charge collection and gain, pulse characteristics and timing resolution for a range of fluences will be presented. In the same section, the performances of the 35 μm and 50 μm thick UFSD (50D) from HPK will be compared.
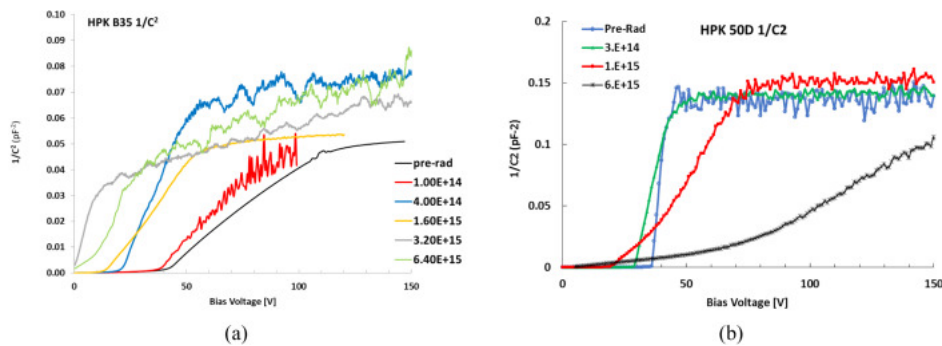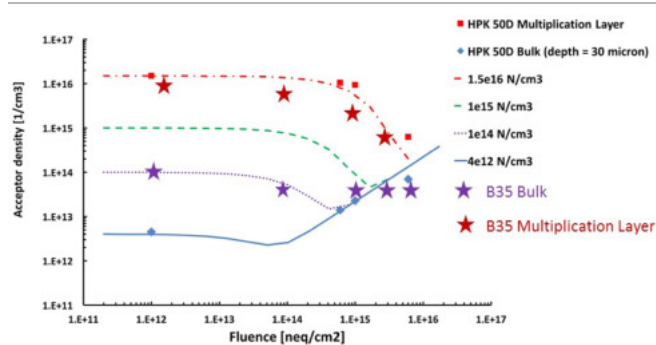
Download high-res image (363KB)   Download full-size image

Fig. 1. 1/C² vs. bias voltage for the 35 μm thin B35 (a) and the 50 μm thin 50D (b) (from [14]) at room temperature before irradiation and at –20 °C after neutron irradiation to the fluences indicated.

2. Properties of the HPK UFSDs B35 (35 μm thick) and 50D (50 μm thick)

The B35 device is a 35 μm thick UFSD sensor from HPK, making it the thinnest UFSD tested in an irradiation campaign to date. The physical thickness including the support wafer is 400 μm. The sensor is 1×1 mm^2, it is not protected by a guard ring and it has a capacitance of 4.6 pF. Its characteristics were measured with I-V and C-V scans before irradiation and after neutron irradiation with fluences $1 \cdot 10^{14}$, $4 \cdot 10^{14}$, $1 \cdot 10^{15}$, $3 \cdot 10^{15}$, $6 \cdot 10^{15}$ neq/cm^2. Gain and time resolution were determined in a β-telescope at UCSC at two temperatures (–20 °C and –27 °C) and the results were compared to the HPK 50 μm thick UFSD 50D reported in [14]. The measuring techniques used in these measurements are explained as well in the same reference. The IV measurements show a current that is below the precision of the power supply for both sensor before irradiation. After irradiation the current was observed to increase with fluence going up to a few μA for the highest fluence.

The C-V measurements can be used to extract changes in the doping profile in both the multiplication layer and the bulk. The C-V measurements were taken at 1 kHz at room temperature and at 200 Hz for the irradiated sensors at –20 C. The frequency was changed between 200 Hz and 2 kHz and the temperature between –20 C and –30 C without changes in the extracted parameter. The C-V curves for the two detectors are shown in Fig. 1 where the 1/C^2 are plotted vs. the bias voltage. The intercept with the bias voltage axis is proportional to the doping density in the multiplication layer, and the slope of the curve to the doping density of the bulk. The effects of acceptor removal in the multiplication layer and the acceptor creation in the bulk are clearly visible by the shortening of the "foot" (the region at low voltage where the 1/C^2 curve appears flat before a sudden increase) and the changes in the subsequent slope.

For the 50D detector (Fig. 1, b), the slope and the length of the "foot" are monotonically decreasing with fluence. For the B35 detectors (Fig. 1, a) the length of the "foot" is about the same up to $1 \cdot 10^{14}$ n/cm^2, following a large decrease at $4 \cdot 10^{14}$. The slope is similar between the pre-irradiation case and the three fluences for the interplay of acceptor creation by deep traps and initial acceptor removal by irradiation [1]. The evolution of the doping densities of the multiplication layer and of the bulk for the 50D and B35 sensors are shown in Fig. 2, overlapped to the model of acceptor creation and removal explained in [1]. One difference between the two sensor types is the initial doping concentration of the bulk: $4 \cdot 10^{13}$ cm^{-3} for 50D and $1 \cdot 10^{14}$ cm^{-3} for B35.
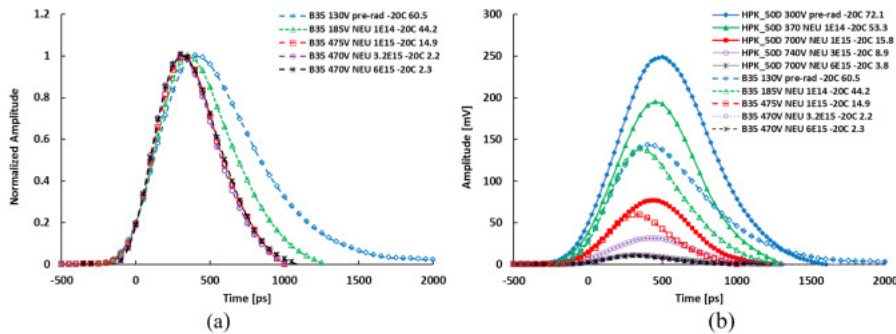

Download high-res image (241KB)   Download full-size image

Fig. 2. The fluence evolution of the doping concentration in the multiplication layer and the bulk for the 35 μm thick B35 and 50 μm thick 50D (taken from [15]). The curves are simulations described in [1] based on data of [16].

3. Neutron irradiations

The UFSD were irradiated without bias in the JSI research reactor of TRIGA type in Ljubljana, which has been used successfully in the past decades to support sensor development [17]. The neutron spectrum and flux are well known and the fluence is quoted in 1 MeV equivalent neutrons per cm^2 (neq/cm^2 or shortened n/cm^2). After irradiation, the devices were annealed for 80 min at 60 °C. Afterward the devices were kept in cold storage at –20 °C.

4. β-telescope setup

The laboratory setup with ^{90}Sr β-source as well as the readout electronics has been previously described in detail in [6], [14], [18]. It is important to note that the system is housed in a climate chamber allowing operations of irradiated sensors at lower temperature down to –27 °C. The trigger and time reference is provided by a second UFSD, which in case of the 50D measurements is a CNM UFSD with a time resolution of 27 ps, while for the B35 measurements it is a HPK UFSD with time resolution of 15 ± 1 ps (both measured at –20 °C). The time resolution for the trigger UFSD was measured pairing two identical UFSDs. Following a trigger, the traces of both trigger and DUT were recorded, with a rate of a few Hz with a digital scope with an analogue bandwidth of 3 GHz and a digitization step of 50 ps.

Download high-res image (483KB)   Download full-size image

Fig. 3. Average normalized pulse shape for B35 (a) and average pulse shapes for B35 and 50D sensors (b). Sensors name, bias voltage fluence, temperature and gain are indicated in the legend.

5. Data analysis

The analysis follows the steps listed in [6]; additional details of the analysis can be found in [14], [18]. The digital oscilloscope records the full voltage waveform of both trigger and DUT in each event, so the complete event information is available for offline analysis.

The normalized average pulse shape for both sensors before and after irradiation can be seen in Fig. 3: the tails present in the B35 pre-rad pulses indicate that the bias voltage was not sufficiently high to saturate the drift velocity, as indicated by Fig. 1(a).

As detailed in [6], [14], [18] the gain is calculated by dividing the integrated pulse area by the trans-impedance of the readout (4700 Ω) to yield the collected charge, which is then divided by the simulated (using WF2) expected charge for a PiN sensor (no charge multiplication) irradiated at the same fluence. This method takes into account the radiation-generated changes in the bulk and isolates the charge multiplication effects in both gain layer and bulk. The parameters for charge collection in WF2 were tuned (Appendix) by measuring the charge collected in FBK (Fondazione Bruno Kessler – Treno IT) PiN 60 μm diodes that were irradiated at different fluences (Fig. A.1), then the collected charge for 35um and 50um PiN diode was simulated. The common systematic error of the gain is 20% mainly due to the uncertainty in the value of the amplifier trans-impedance.

The time of arrival of a particle is defined with the constant fraction discriminator (CFD) method [14], [18], offering a very efficient correction to the time walk effect. The CFD value can be optimized for every bias voltage and fluence to minimize the time resolution, a procedure that is necessary since both the pulse shape and the noise contributions change with fluence. Due to the oscilloscope digitization steps, the time of arrival at a specific CFD fraction is evaluated with a linear interpolation. The event selection is straightforward: for a valid trigger pulse (passing a 15 mV threshold in amplitude), the signal amplitude (Pmax) of the DUT UFSD should not be saturated by either the scope or the read-out chain. To eliminate the contributions from non-gain events or noise, the time of the pulse maximum (Tmax) has to fall within a window of 1 ns centered on the CFD threshold of 20% of the trigger. The DUT time resolution is calculated from the σ value of the Gaussian fit to the time difference Δt between the DUT and the trigger.
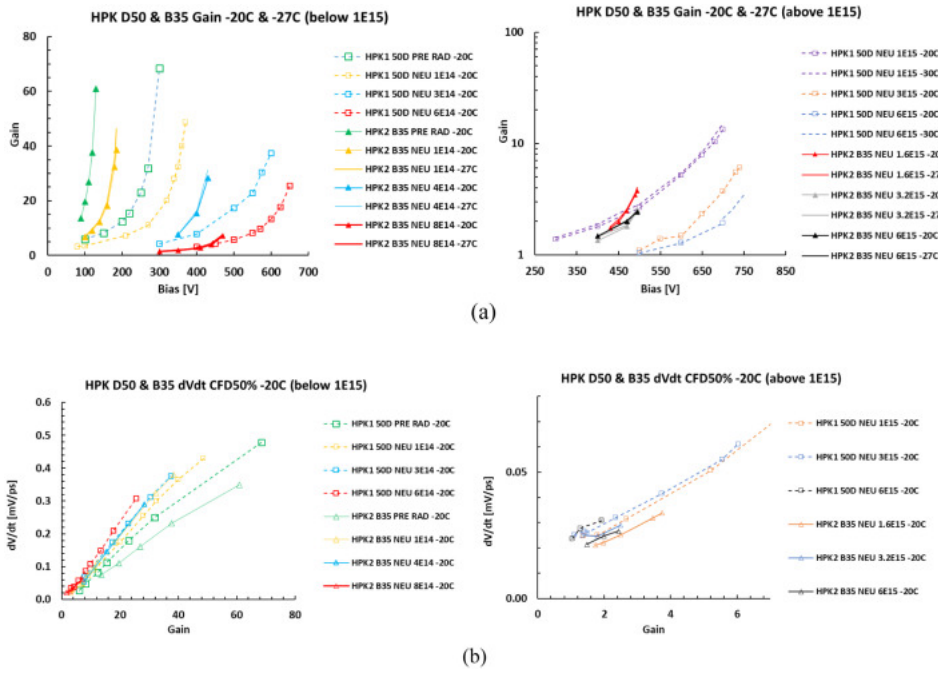
[Download high-res image (605KB)](#)   [Download full-size image](#)

Fig. 4. (a) Gain as a function of bias and (b) slope dV/dt (at CFD 50%) as a function of gain for HPK sensors B35 and 50D for different fluences. As seen in Fig. 1(a), Fig. 3(a) for the B35 sensor before irradiation the bias voltage is too low to achieve saturated drift velocity in the bulk.
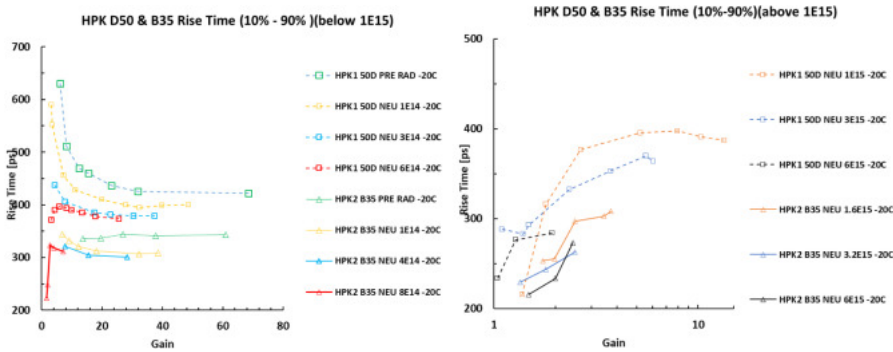
[Download high-res image (294KB)](#)   [Download full-size image](#)

Fig. 5. Rise time as a function of gain for sensors B35 and 50D (–20 C).

6. Results on irradiated 35 μm thick UFSD HPK B35

The timing resolution σ_t can be parameterized as:

$$\sigma_t^2 = \sigma_{Jitter}^2 + \sigma_{Distortion}^2 + \left(\sigma_{Ion\_Amplitude} + \sigma_{Ion\_Uniformity}\right)^2, \tag{1}$$

- In this analysis, since the pad size is much larger than the sensor thickness, distortion effects due to weighting field fluctuations are small and the term $\sigma_{Distortion}^2$ can be ignored.

- The Jitter depends on the ratio between the noise RMS (N in the equation) and the signal voltage slope dV(t)/dt. The signal slope can be approximated to S/t_{rise}, where S is the signal voltage amplitude and t_{rise} the rise time. Finally the amplitude S is also proportional to the gain G. This is shown in Eq. (2):

$$\sigma_{Jitter} = \frac{N}{dV/dt} \approx \frac{t_{rise}}{\frac{S}{N}} \sim t_{rise}\frac{N}{G}. \tag{2}$$

- The terms $\sigma_{Ion\_Amplitude}$, $\sigma_{Ion\_Uniformity}$ originates from the Landau fluctuations in the ionization profile lead two different effects: (i) *Timewalk*, the apparent early arrival of larger signals, mostly due to the variation of the total ionization, and (ii) *LandauNoise*, the variation of the signal time of arrival due to the non-uniformity of the ionization profile. Since large local ionizations causes both $\sigma_{Ion\_Amplitude}$, $\sigma_{Ion\_Uniformity}$ to increase, the two effects are not uncorrelated. Techniques such as Constant Fraction Discrimination (CFD) or Time-over-Threshold (ToT) are used to correct the time walk contribution, so the *Timewalk* term can be eliminated. We use the term *Landau Noise* to identify the contributions to the time resolution of the remaining terms due to Landau fluctuations:

$$\left(\sigma_{Ion_{Amplitude}} + \sigma_{Ion_{Uniformity}}\right)^2 = \sigma^2_{\_IonAmplitude} + \sigma^2_{\_Ion\_Uniformity} \qquad (3)$$
$$+ 2\sigma_{Ion\_Amplitude} * \sigma_{Ion\_Uniformity} \sigma^2_{LandauNoise} = \sigma^2_{Ion\_Uniformity}$$
$$+ 2\sigma_{Ion\_Amplitude} * \sigma_{Ion\_Uniformity}$$

To reduce the jitter contribution below the Landau noise the gain needs to be large, above 15–20. A comparison of the voltage dependence of the gain (Fig. 4(a)) shows that B35 requires a lower bias voltage than 50D for the same gain, and that the bias voltage gap between the two sensors of ∼ 200 V (at the same gain value) is approximately preserved through the radiation steps. The strong dependence of the signal slope dV/dt (measure as the slope between two points near the chosen CFD percentage) on the gain is shown in Fig. 4(b), which shows little difference between the two detector types with the exception of the B35 sensors before radiation, where the bias voltage was too low to achieve saturated drift velocity in the bulk yielding to higher drift time. As shown in the C-V curve (Fig. 1(a)), the bias voltage reached for this sensor is not or only barely sufficient to deplete the sensor, and thus causes a reduction in the slope. Since the noise of the two sensor types is very similar as expected using similar amplifier readout boards, for the same gain the jitter contribution to the resolution should scale with the detector thickness.

Another parameter determining the time resolution is the rise time. As expected the rise time (Fig. 5) for the **35 μm** thick detector is significantly shorter than for the **50 μm** detector at all fluences. In both sensors the rise time decreases with irradiation.

Fig. 6 shows the CFD scan of the time resolution for B35 and 50D while keeping the trigger sensor at the fixed CFD of 20%. The optimal range for the CFD fraction, defined as the range to be within 10% of the minimum time resolution, is for B35 before irradiation: 7%–36% while after $1 \cdot 10^{14}$ is 12%–90%, after $4 \cdot 10^{14}$: 11%–96%, after $1 \cdot 10^{15}$: 15%–99%, after $3 \cdot 10^{15}$: 25%–95%, and after $6 \cdot 10^{15}$ neq/cm^2: 35%–95%. These numbers indicate a very flat dependence of the time resolution on the CFD fraction for B35. For 50D the optimal CFD range tends to be narrower.
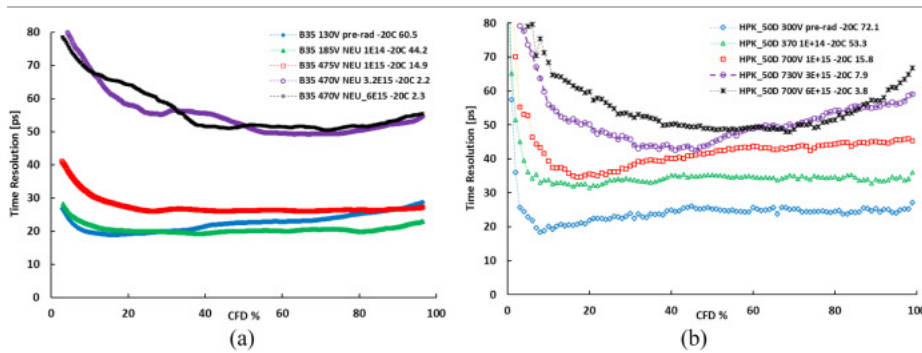
Download high-res image (430KB)   Download full-size image

Fig. 6. CFD scan at optimum operating voltage for sensors B35 (a) and 50D (b). The legends are bias, fluence, temperature, gain.
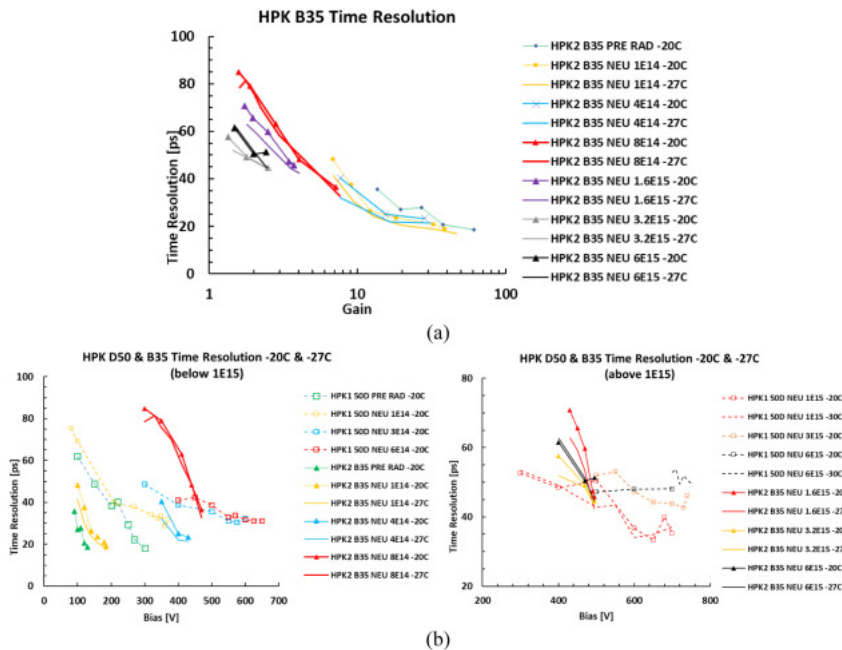
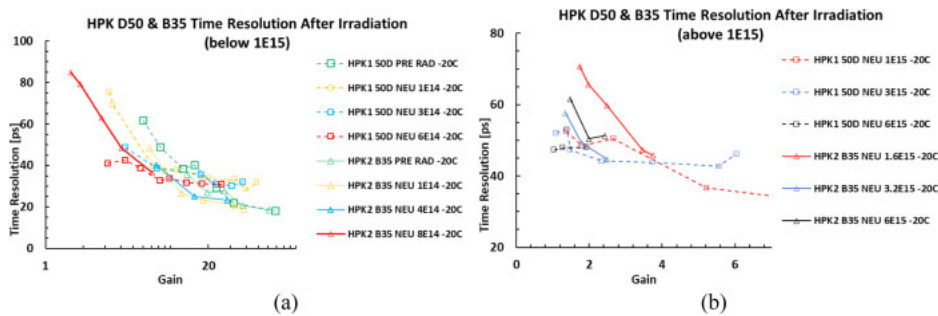Download high-res image (550KB)   Download full-size image

Fig. 7. Time resolution as a function of gain for B35 (a) and bias voltage (b) for sensors B35 and 50D. The values are for the CFD optimized for the optimal time resolution.

The time resolution as a function of gain and bias voltage for different fluences can be found in Fig. 7. It can be seen that the B35 detector requires lower bias, and until irradiation up to $8 \cdot 10^{14}$ n/cm^2 has superior time resolution when compared to 50D. Furthermore it was observed that B35 shows a small improvement in time resolution going from –20 °C to –27 °C (Fig. 9(b)).

In Fig. 8 the time resolution for B35 and 50D is shown as a function of gain before (a) and after irradiation (b). We expect that at large gain the resolution has a constant value limited by Landau fluctuations, which is smaller for **35** μ**m** than for **50** μ**m** UFSD. This is indeed true for the irradiated sensors on Fig. 7(b), while this fact could not be measured before irradiation due to the low bias voltage of B35 which limits the drift velocity of the electrons and holes to sub-optimal values.

For low gain, where the jitter is the dominant contribution to the resolution (cf. Fig. 4(b) and Eq. (2)), the difference between the two thicknesses are indeed small.
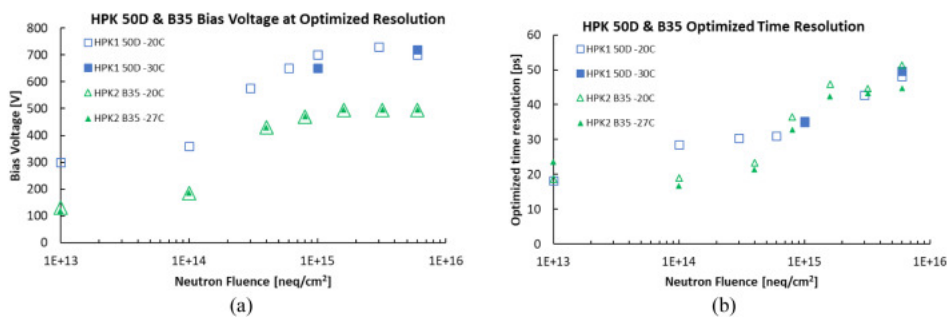
The time resolutions as a function of fluence are presented in Fig. 9. The optimal CFD fraction used for B35 is 26% before irradiation, 43% after $1 \cdot 10^{14}$, 35% after $4 \cdot 10^{14}$, 40% after $1 \cdot 10^{15}$, 60% after $3 \cdot 10^{15}$, and 70% after $6 \cdot 10^{15}$ neq/cm^2 while for 50D it is 8% before irradiation, 20% after $1 \cdot 10^{14}$, 20% after $1 \cdot 10^{15}$, 48% after $1 \cdot 10^{15}$ and 54% after $1 \cdot 10^{15}$ neq/cm^2.

Fig. 8. Time resolution as a function of gain for B35 and 50D for low (a) and high (b) irradiation.

Fig. 9. (a) Optimum operating voltage and (b) time resolution as a function of fluence for sensors B35 and 50D.

We define as the optimum operating voltage (shown in Fig. 9(a)) as the lowest bias voltage at which the time resolution using the optimal CFD threshold is smallest. After a fluence of $1 \cdot 10^{15}$ neq/cm^2 the bias voltages required are 500 V (B35) and 700 V (50D). The difference in bias and thickness influences the power dissipation. In order to reach a time resolution of 33 ps, 50D will dissipate four times the power than B35.

Fig. 9(b) shows the improvement of the time resolution of the **35** μ**m** thick B35 over the **50** μ**m** thick 50D. Up to a fluence of $4 \cdot 10^{14}$ n/cm^2 the time resolution is below 25 ps, about 10 ps lower than for the **50** μ**m** thick 50D

7. Conclusions

Two UFSD from Hamamatsu Photonics with respective thickness of **35** μ**m** (B35) and **50** μ**m** (50D) were tested using a ^{90}Sr β-telescope after neutron irradiation up to $6 \cdot 10^{15}$ n/cm^2. The operating bias for the B35 sensor is about 200 V lower than that of the 50D sensor.

The CFD scans of B35 reveal an almost flat dependence of the time resolution on the CFD fraction. A constant CFD fraction of about 50% will result in a satisfactory time resolution for all fluences.

The two detectors show similar time resolution before irradiation: 19 ps for B35 vs. 18 ps for 50D (tested at –20 °C). Here the operating bias for B35 is close to depletion. After a neutron fluence of $1.6 \cdot 10^{15}$ n/cm^2 at –20 °C, the time resolution for B35 is 36 ps and for 50D 35 ps, and at –27 °C B35 has a time resolution of 33 ps compared with 35 ps for 50D at –30 °C.

At higher neutron fluence than $1.6 \cdot 10^{15}$ n/cm^2 B35 has slightly worse resolution than 50D because of smaller charge. The performance after large fluences is limited by the breakdown voltage of the UFSD. Since at lower fluence the resolution is limited by the Landau fluctuations and at higher fluences by the jitter, an improved time resolution might be expected for larger fluences by extending the bias reach of the **35** μ**m** thick sensors without increasing the noise. This will be an important prototyping goal for the UFSD.

The B35 sensor shows a dissipated power that is significantly less than the power dissipated by the 50D sensor. After a fluence of $1.6 \cdot 10^{15}$ n/cm^2, to reach a resolution of 33 ps, 50D dissipates 4 times the power than B35.

UFSD of **35** μm thickness are thus good candidates for the use in the ATLAS and CMS upgrade projects for the HL-LHC.
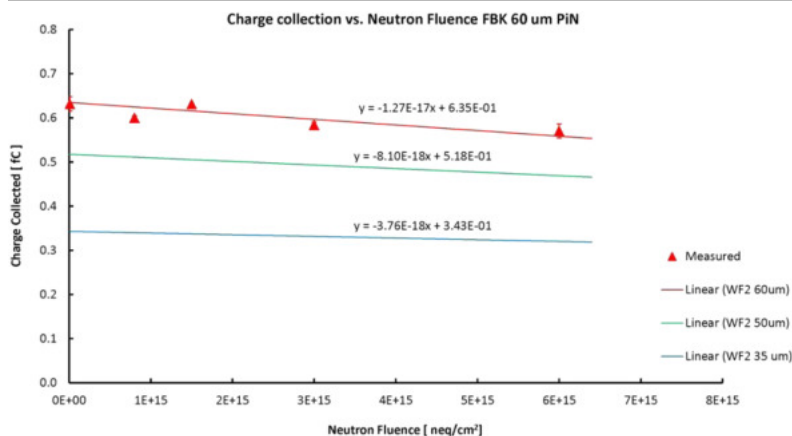
Acknowledgments

Appendix. Gain calculation

See Fig. A.1.

Download high-res image (209KB)　　　　Download full-size image

Fig. A.1. Collected charge for 60 μm FBK PiN diodes (red triangles) for different irradiation fluences. The colored lines shows the WF2 simulation with parameters tuned to reproduce the 60 μm PiN data. The simulation for 35 μm and 50 μm PiN diode was used to calculate the gain for B35 and 50D respectively.

Special issue articles　　　　Recommended articles　　　　Citing articles (1)

References

[1]　Sadrozinski H.F.-W., Seiden A., Cartiglia N.
4D tracking with ultra-fast silicon detectors
Rep. Progr. Phys., 81 (2018), p. 026101
CrossRef　　　Google Scholar

[2]　Pellegrini G., *et al.*
Technology developments and first measurements of Low Gain Avalanche Detectors (LGAD) for high energy physics applications
Nucl. Instrum. Methods A, 765 (2014), p. 24
Google Scholar

[3]　Sadrozinski H.F.-W., *et al.*
Ultra-fast silicon detectors
Nucl. Instrum. Methods A, 831 (2016), p. 18
Article　　　Download PDF　　　View Record in Scopus　　　Google Scholar

[4]　M. Carulla, et al. First **50**μm thick LGAD fabrication at CNM, 28th RD50 Workshop, Torino, June 7th 2016,
https://agenda.infn.it/getFile.py/access?contribId=20&sessionId=8&resId=0&materialId=slides&confId=11109.
Google Scholar

[5]　RD50 collaboration, http://rd50.web.cern.ch/rd50/.
Google Scholar

[6]　Cartiglia N., *et al.*
Beam test results of a 16 ps timing system based on ultra-fast silicon detectors
Nucl. Instrum. Meth., A850 (2017), pp. 83-88
Article　　　Download PDF　　　View Record in Scopus　　　Google Scholar

[7]   Cartiglia N., *et al.*
        Performance of ultra-fast silicon detectors
        JINST, 9 (2014), p. C02001
        CrossRef   Google Scholar

[8]   Cartiglia N.
        Design optimization of ultra-fast silicon detectors
        Nucl. Instrum. Methods A, 796 (2015), pp. 141-148
        Article   Download PDF   View Record in Scopus   Google Scholar

[9]   Cenna F., *et al.*
        Weightfield2: a fast simulator for silicon and diamond solid state detector
        Nucl. Instrum. Meth, A796 (2015), p. 149
        http://personalpages.to.infn.it/cartigli/Weightfield2/Main.html
        Article   Download PDF   View Record in Scopus   Google Scholar

[10]   HL-LHC, http://dx.doi.org/10.5170/CERN-2015-005.
        Google Scholar

[11]   L. Gray, 4D Trackers, at Connecting the dots, Paris 2017,
        https://indico.cern.ch/event/577003/contributions/2476434/attachments/1422143/2180715/20170306_LindseyGray_CDTWIT.pdf.
        Google Scholar

[12]   G. Kramberger, et al. Radiation hardness of thin LGAD detectors, TREDI 2017,
        https://indico.cern.ch/event/587631/contributions/2471705/attachments/1414923/2165831/RadiationHardnessOfThinLGAD.pdf.
        Google Scholar

[13]   J. Lange, et al. Gain and time resolution of $45\mu m$ thin LGAD before and after irradiation up to a fluence of 10^{15}neq/cm^2, JINST, 12 P05003.
        Google Scholar

[14]   Z. Galloway, et al. Properties of HPK UFSD after neutron irradiation up to 6e15 n/cm^2 arXiv:1707.04961.
        Google Scholar

[15]   Kramberger G., *et al.*
        Radiation effects in low gain avalanche detectors after hadron irradiations
        JINST, 10 (2015), p. P07006
        CrossRef   Google Scholar

[16]   Kramberger G., *et al.*
        Effective trapping time of electrons and holes in different silicon materials irradiated with neutrons
        protons and pions, Nucl. Instrum. Methods Phys. Res. A, 481 (2002), pp. 297-305
        Article   Download PDF   View Record in Scopus   Google Scholar

[17]   Snoj G.ˇZerovnik, Trkov A.
        Computational analysis of irradiation facilities at the JSI TRIGA reactor
        Appl. Radiat. Isot., 70 (2012), p. 483
        Google Scholar

[18]   Y. Zhao, UCSC Senior Thesis 2017, https://drive.google.com/drive/folders/0ByskYealR9x7bFY1ZS1pZW9SRWs.
        Google Scholar

[1]   Permanent address: INFN, Torino, Italy.